

# Analysis and visualization of spatial transcriptomic data

Boxiang Liu<sup>1\*</sup> and Yanjun Li<sup>1</sup>

<sup>1</sup>Baidu Research, Sunnyvale, CA, USA, 94089

## Abstract

Human and animal tissues consist of heterogeneous cell types that organize and interact in highly structured manners. Bulk and single-cell sequencing technologies remove cells from their original microenvironments, resulting in a loss of spatial information. Spatial transcriptomics is a recent technological innovation that measures transcriptomic information while preserving spatial information. Spatial transcriptomic data can be generated in several ways. RNA molecules are either measured by *in situ* sequencing, *in situ* hybridization, or spatial barcoding to recover original spatial coordinates. The inclusion of spatial information expands the range of possibilities for analysis and visualization, and spurred the development of numerous novel methods. In this review, we summarize the core concepts of spatial genomics technology, and provide a comprehensive review of current analysis and visualization methods for spatial transcriptomics in the expression domain, spatial domain, and interaction domain.

## 1 Introduction

Quantification of gene expression has important applications across various aspects of biology. Understanding the spatial distribution of gene expression has helped to answer fundamental questions in developmental biology (1, 2), pathology (3, 4), cancer microenvironment (5-8), and neuroscience (9-11). Two widely used methods for gene expression quantification are fluorescent *in situ* hybridization (FISH) and next-generation sequencing. With FISH, fluorescently-labeled RNA sequences are used as probes to identify its naturally occurring complementary sequence in cells, while preserving the spatial location of the target sequences (12). Traditionally, the number of target sequences simultaneously identified by *in situ* hybridization is restricted by the number of fluorescent channels, making this method suitable for targeted gene detection. On the other hand, next-generation sequencing methods use a shotgun approach to quantify RNA molecules across the entire transcriptome (13). To achieve transcriptome-wide quantification, RNA must be first isolated and purified, which removes RNA molecules from their native microenvironment. Even with single-cell sequencing, where the cellular origin of RNA molecules is preserved, spatial information of cells can only be inferred but not directly measured (14, 15).

Integration of spatial information with transcriptome-wide quantification has given rise to the emerging field of spatial transcriptomics. Currently, spatial transcriptome quantification falls into three broad categories (Table 1). First, spatial barcoding methods ligate oligonucleotide barcodes with known spatial locations to RNA molecules prior to sequencing (16-22). Both barcodes and RNA molecules are jointly sequenced and spatial information of sequenced RNA molecules can be recovered from associated barcodes. Second, *in situ* hybridization methods coupled with combinatorial indexing can vastly increase the number of RNA species identified (23-26). The latest *in situ* hybridization methods can detect around 10,000 RNA species from a given sample (23). Third, *in situ* sequencing method uses fluorescent-based direct sequencing to read out base pair information from RNA molecules in their original spatial location (27, 28).

\*Correspondence: jollier.liu@gmail.com

Several metrics need to be considered when selecting a method for a specific application (Table 1). Methods employing *in situ* hybridization provide subcellular resolution. Leveraging super-resolution microscopy, *in situ* hybridization methods can achieve a resolution of ~10nm, sufficient to distinguish single RNA molecules (29). In addition, *in situ* methods require no PCR amplification of cDNA, thus avoiding amplification bias. However, the number of RNA species detected by *in situ* methods is limited by the indexing scheme, which is currently limited to ~10,000 genes but will likely improve in the future. Furthermore, the area examined by *in situ* methods is limited by the field-of-view of the microscope objective lens. In contrast, spatial barcoding followed by shotgun sequencing can in principle sample the whole transcriptome. This is ideal if the target molecules are unknown *a priori*. Spatial barcoding can also examine larger tissue areas, making it ideal for larger samples such as the brain. However, spatial resolution of current spatial barcoding methods is limited by the density of measurement spots, which can range from multicellular to subcellular. In addition, shotgun sequencing inevitably suffers from PCR amplification bias (30), as well as “dropout” when sequencing read depth is insufficient (31). Thus far, we have provided an overall picture of different spatial transcriptomic methods and their characteristics. Because this review focuses on analysis and visualization of spatial transcriptomics, readers who wish to understand the experimental details can refer to comprehensive reviews elsewhere (32).

**Table 1:** Current experimental methods for spatial transcriptomic profiling

Method	Type	Resolution	Genes	Reference
<b>Visium</b>	Spatial barcoding	55µm	Whole transcriptome	(16)
<b>Slide-seq</b>	Spatial barcoding	10µm	Whole transcriptome	(17, 18)
<b>HDST</b>	Spatial barcoding	2µm	Whole transcriptome	(19)
<b>DBiT-Seq</b>	Spatial barcoding	10µm	Whole transcriptome	(20)
<b>Seq-scope</b>	Spatial barcoding	0.6µm	Whole transcriptome	(21)
<b>Stereo-seq</b>	Spatial barcoding	500nm	Whole transcriptome	(22)
<b>seqFISH</b>	<i>in situ</i> hybridization	single-molecule	>10,000	(23, 24)
<b>merFISH</b>	<i>in situ</i> hybridization	single-molecule	100 – 1,000	(25, 26)
<b>STARmap</b>	<i>in situ</i> sequencing	single-cell	160 – 1020	(27)
<b>FISSEQ</b>	<i>in situ</i> sequencing	subcellular	~ 8000	(28)

The following sections are organized by analysis and visualization techniques (Figure 1). Section 2 briefly discusses preprocessing of spatial transcriptomic data, an essential step prior to any analysis or visualization. Section 3 dissects methods whose outputs are visualized in the gene expression domain and independent of spatial coordinates. This includes dimensionality reduction, clustering, and cell type identification. Section 4 describes methods whose outputs are visualized with spatial coordinates. This includes identification of spatially coherent gene expression patterns and identification of spatial domains. Section 5 describes methods whose outputs involve the interaction between cells or genes. This includes the identification of cell-to-cell communication and gene interaction.

## 2 Preprocessing

Spatial transcriptomic datasets add a new dimension to transcriptomic analyses. Spatial coordinates of cells enable novel analyses such as spatial differential expression (33) and cell-cell interaction (34). Similar to single-cell RNA-seq datasets, a spatial transcriptomic dataset can be represented by a gene-by-cell count matrix. A second matrix of coordinates is attached to the cell dimension of the count matrix to represent spatial information. Various preprocessing steps may be performed prior to any analysis. First, genes and cells may be filtered based on threshold specific to the dataset. For example, a cell may be removed if less than 1,000 genes have non-zero counts, and a gene may be removed if it is detected in less than 10 cells (35). Cells with a high proportion of mitochondria RNA may be removed due to the loss of cytoplasmic RNA (36). Transformation of count data may be performed according to downstream modeling assumptions. Methods that model raw counts do not require any transformation (37). Otherwise, gene expression per cell may be normalized to have the same total library size so that expression levels are comparable across cells. The gene expression matrix may then be log-transformed and be regressed against confounders such as batch effect, percentage of mitochondria genes, and other technical variations. Although preprocessing steps mentioned above are widely adopted, the exact configuration should follow input data modality and modeling assumptions, and there is no one-size-fits-all strategy. Sections below assume data are preprocessed and analysis-ready.

## 3 Analysis and visualization in the expression domain

A first step in the spatial transcriptomic analysis is to identify the cell type (for datasets of single-cell resolution) or cell mixture (for datasets of multicellular resolution) of each spatial unit or spot. Cell type identification usually starts with dimensionality reduction technique to reduce time and space complexity for downstream analysis. The reduced representations are used to cluster cells based on the assumption that cell of the same type falls into the same cluster.

### 3.1 Clustering

The selection of clustering techniques is critical for obtaining good clustering results. Certain methods with assumptions about cluster shapes may not be suitable for spatial genomic data. For example, K-means clustering assumes that the shapes of clusters are spherical and that clusters are approximately of the same size (38), and Gaussian mixture models assume that points with each cluster follow a Gaussian distribution (39). These assumptions are rarely satisfied by spatial transcriptomic data.

Agglomerative clustering methods are a class of methods that iteratively aggregate data points into clusters. These methods do not carry assumptions about the shape and size of clusters. At each iteration, data points are aggregated to optimize a pre-defined metric. Popular agglomerative clustering methods include hierarchical agglomerative clustering (40) and community detection methods such as Louvain (41) and Leiden (42) algorithms. Hierarchical agglomerative clustering is initialized by treating each

point as its own cluster. Each iteration aggregates two clusters with the closest distance to form a new cluster until no clusters can be merged. Popular distance metrics include single linkage (distance between two closest points from two clusters), complete linkage (distance between two farthest points from two clusters), average linkage (average pairwise distance between all points from two clusters), and centroid linkage (distance between two cluster centroids) (43). The optimal linkage metric varies between datasets and is specified by the user.

Community detection methods, i.e., Louvain (41) and Leiden (42) algorithms, have seen wide adoption in the single cell and the spatial transcriptomics community. Both algorithms try to iteratively maximize the modularity metric defined below:

$$H = \frac{1}{2m} \sum_c \left( e_c - \frac{K_c^2}{2m} \right)$$

where  $m$  is the total number of edges in the graph;  $K_c$  is the sum of degrees for all nodes in cluster  $c$ ;  $e_c$  is the total number of edges in cluster  $c$ . Intuitively, a tightly connected community or cluster should have a large number of observed edges ( $e_c$ ) relative to the expected number of edges ( $K_c/2m$ ). The Louvain algorithm is initialized by assigning each node to its own community. At each iteration, each node moves from its own community to all neighboring communities and changes in  $H$  are calculated. The node is moved to the community, which results in the largest increase in  $H$ . At the end of each iteration, a new network is built by aggregating all nodes within the same community, and a new iteration begins. The procedure will terminate when the increase in  $H$  can no longer be achieved.

### 3.2 Identification of cell types

Identification of cell types starts by defining cell-type specific genes or marker genes. A straightforward approach is to perform differential expression analysis (44, 45) between all pairs of clusters. Genes that are consistently over-expressed in one cluster are considered its marker genes. This is the approach implemented in scran (36) and Mast (46).

Another method, scGeneFit, uses a label-aware compression method to find marker genes (47). Given cell-by-gene expression matrix and corresponding cell labels inferred from clustering results, scGeneFit find a projection onto a lower-dimensional space, in which cells with the same labels are closer in the lower-dimensional space than cells with different labels. The projection is constrained such that the axes in the lower-dimensional space align with a single gene. Therefore, the marker genes will be the set of axes in the lower-dimensional space that best conserves label structures. The marker genes can then be matched with an expert-curated list of cell-type specific genes to infer cell types (48, 49).

Unlike the above approaches, JSTA uses deep learning for cell type identification and incorporates three distinct and interactive components: a segmentation map and two deep neural network-based cell type classifiers for pixel-level and cell-level classification (50). JSTA first trains a taxonomy-based cell-level classifier with the external data from the Neocortical Cell Type Taxonomy (NCTT) set (51). Then the segmentation map and pixel-level classifier are iteratively refined with an expectation-maximization (EM) algorithm. Specifically, the segmentation map is initialized by a classical image segmentation algorithm watershed (52) and paired with the trained cell-level type classifier to predict the current cell (sub)types. Given the local mRNA density at each pixel as the input, the pixel-level classifier is optimized to closely match each pixel's current cell type assignment. Next, the updated pixel-level classifier reclassifies the cell types of all border pixels, and the resulting segmentation map

requires an update of the cell-level classification, which further triggers an update of pixel-level classifier training. This learning process is repeated until convergence. The eventual segmentation map tends to maximize consistency between local RNA density and cell type expression priors.

### 3.3 Visualization of gene expression in low dimensions

The identified clusters can be visualized to ensure cells assigned to the same cluster are close in expression space. Dimensionality reduction techniques are necessary to project the high dimensional data into 2D or 3D. Principal component analysis (PCA) is widely adopted in the single cell and spatial transcriptomic literature (53). This method identifies linear combinations of the original dimensions, or principal components (PC), that maximize the variance of projection from data points onto the principal components. The principal components can be computed in an iterative way: the first PC can point in any direction to maximize variance of projections, and each subsequent PCs are orthogonal to previous PCs (54).

In contrast to PCA, manifold learning is a class of non-linear dimensionality reduction techniques that aims to project the data to a lower dimension while maintaining the distance relations in the original high-dimension space; points close to each other in the original space will be close in the low-dimensional space. Uniform manifold approximate and projection (UMAP) and t-distributed stochastic neighbor embedding (t-SNE) are two manifold learning methods widely adopted in single cell and spatial transcriptomic literature (55, 56). Both methods follow a two-step procedure. In the first step, a similarity matrix is computed based on a pre-defined distance metric. In the second step, all data points are placed in a low-dimensional Euclidean space such that the structure of the similarity matrix is preserved. This step is initialized by randomly placing data points in the low-dimensional space. At each iteration, data points are moved according to the similarity matrix from the high-dimensional space; points with high similarity in the high-dimensional space will attract and those with low similarity will repel. Because optimization is done iteratively, UMAP and t-SNE results are stochastic and will vary between runs. Random seeds are needed for reproducibility. The two methods differ in their construction of similarity matrix. In t-SNE, a distance matrix is calculated according to probability density functions (PDF) of the Gaussian distribution in the high-dimension space, and PDFs of the t-distribution in the low-dimension embedding. In UMAP, an adjacency matrix is constructed by extending a sphere whose radius depends on the local density of nearby points; two points are connected if their spheres overlap. In practice, UMAP is faster than t-SNE and tends to better preserve the high-dimensional structure.

## 4 Analysis and visualization in the spatial domain

An important question in spatial transcriptomic data analysis is to identify gene whose expression follows a coherent spatial pattern. Genes with spatial expression patterns are important determinants of polarity and anatomical structures. For example, the gene *wingless* is a member of the *wnt* family that plays a central role in anterior-posterior pattern generation during the embryonic development of *Drosophila melanogaster*. The gene is expressed in alternating stripes across the entire embryo (57). Another example is the neocortex of mammalian brains, which contain six distinct layers. Each layer consists of different types of neurons and glial cells that express cell-type specific marker genes (58). Spatial transcriptomic data enables unbiased transcriptome-wide identification of spatially expressed genes, but it is excessively labor-intensive to visually examine all genes. This prompted the development methods including SpatialDE (33), trendsseek (59), and Spark (37).

### 4.1 Identifying genes with spatial expression patterns

SpatialDE (33) uses a Gaussian process to model gene expression levels. Intuitively, a Gaussian process model treats all data points as observations from a random variable that follows a multivariate Gaussian (MVN) distribution (60). To test whether expression levels follow a spatial pattern, the authors specify a null model, in which the covariance matrix is diagonal, and an alternative model, in which the covariance matrix follows a radial basis function kernel:

$$K(x_i, x_j) = \exp(-\gamma \|x_i - x_j\|^2)$$

where  $K(x_i, x_j)$  is the covariance between i-th and j-th measurement;  $x_i$  and  $x_j$  represent the spatial coordinates of the i-th and the j-th measurement;  $\gamma$  is a scale factor. Intuitively, the Gaussian kernel describes a spatial relationship in which nearby points have similar expression values. This kernel assumes that cells of similar origins tend to neighbor each other in space. A likelihood ratio test can be done by comparing the likelihood of the null and the alternative model. Because SpatialDE is a Gaussian process model, the expression values must be log-transformed which decreases power.

Trendsseek (59) uses a marked point process model in which each point of measurement, or a spot, is treated as a point process and each point is marked with a gene expression value. To decide whether a gene whose expression follows a spatial pattern, trendsseek test whether the probability of finding two marks given the distance between two points deviates from what would be expected if the marks were randomly distributed over points. To calculate the null distribution given no spatial pattern, trendsseek implements a sampling procedure in which marks are permuted with location of points fixed. In practice, such sampling procedure is computationally expensive and makes trendsseek only suitable for small datasets.

Spark (37) uses a generalized linear spatial model (GLSM) to directly model count data (61, 62), which results in better power than SpatialDE. A simplified model is presented below:

$$\begin{aligned} y(s) &\sim \text{Poisson}(\lambda(s)) \\ \log(\lambda(s)) &= x(s)^T \beta + b(s) + \epsilon \\ b(s) &\sim \text{MVN}(0, \tau K(s)) \end{aligned}$$

Where  $y(s)$  is the gene expression of sample  $s$ .  $\lambda$  is a Poisson rate parameter, which is modeled as a linear combination of three terms. The first term  $x(s)$  represents covariates such as batch effect and library size for sample  $s$ . The second term  $b(s)$  is the spatial correlation pattern modeled as a Gaussian process. The last term  $\epsilon$  is random noise. To determine whether a gene follows a spatial pattern, Spark tests whether  $\tau = 0$ . Parameter estimation is difficult due to the random effects terms. *Monte Carlo* methods are the gold standard for parameter estimation for GLSM but are computationally expensive. Instead, the authors developed a penalized quasi-likelihood (PQL) estimation procedure to make computation tractable for large datasets (62-64). Spark produces well-calibrated p-values and is more powerful than trendsseek and SpatialDE through a series of simulation experiments.

## 4.2 Identification of spatial domains

Spatially coherent domains often underly important anatomical regions. A motivating example is the histological staining of cancer tissue slides. Cancer regions and normal tissues can be visually distinguished due to differential affinities to staining agents. This enables pathologists to grade and stage individual cancer tissue slides according to the location and size of the cancer regions (65). Spatial

transcriptomics enables histology-like identification of spatial domains. Regular histology slides can be visualized conveniently with RGB pixels. In contrast, spatial transcriptomic data cannot be directly visualized because each spot (i.e., pixel) in spatial transcriptomic data has dimension equal to the number of genes. This prompts the development of methods to detect spatial domains, including BayesSpace (66), SpatialDE (33), and a hidden Markov random field (HMRF) method (67).

The three methods share a common assumption that hidden spatial domains can be described by latent variables, which are not directly observed but can be inferred from observed gene expression values. However, these methods use different modeling assumptions to infer latent variables. Zhu et al. (67) developed an HMRF-based method, a widely adopted model in the image processing community to identify patterns in 2D images (68, 69), to identify spatial domains. An HMRF has two components: it uses a Markov random field to describe the joint distribution of latent variables, and a set of observed examples that depends on them. The latent variables are assumed to satisfy the Markov property, in which any node in the network is conditionally independent of other nodes given its neighbors. Following this assumption, a Markov random field of latent variables can be decomposed into a set of subgraphs, called cliques, which gives rise to the observed gene expression. The parameters of the model by Zhu et al. are estimated with an EM algorithm (70, 71).

Both SpatialDE (33) and BayesSpace (66) models the observed gene expression values as a mixture of Gaussian random variables. The means of the Gaussian random variables are determined by the spatial domain membership. In SpatialDE, the mean expression value of each spatial domain is described by a Gaussian process, whose covariance follows a radial basis function kernel. The observed expression follows a Gaussian distribution centered around the mean expression value of a given spatial domain. The posterior distribution of parameters and the latent spatial domain membership is estimated by variational inference. Different from SpatialDE, BayesSpace uses a diagonal matrix to model the covariance of the mean expression of each spatial domain. The observed gene expression is modeled as a Gaussian random variable centered around the mean expression and has a diagonal covariance matrix modeled as a Wishart random variable. BayesSpace uses a Markov chain Monte Carlo (MCMC) method to estimate model parameters (72).

While the above methods consider spatial genes and spatial domain as two separate tasks, SpaGCN proposed a graph convolutional network-based (GCN) approach to address these two tasks jointly (73). With the integration of gene expression, spatial location, and histology information, SpaGCN models spatial dependency of gene expression for clustering analysis of spatial domains and identification of domain enriched spatial variable genes (SVG) or meta genes. SpaGCN first converts the spatial transcriptomics data into an undirected weighted graph of spots, and the graph structure represents the spatial dependency of the data. Next, a GCN (74) is utilized to aggregate gene expression information from the neighboring spots and update every spot's representation. Then, SpaGCN adopts an unsupervised clustering algorithm (75) to cluster the spots iteratively, and each identified cluster will be considered as a spatial domain. The resulting domains guide the differential expression analysis to detect the SVG or meta genes with enriched expression patterns in the identified domains.

### 4.3 Visualization in Euclidean space

After obtaining spatial genes and domains, visualization in the Euclidean space is relatively straightforward. Spatial genes can be visualized by plotting their log-transformed expression values. Spatial domains can be colored by mean expression values, or by their identities (Figure 3). Several packages such as Giotto (76), Scanpy (35), Seurat (77), and Squidpy (78) provides functionalities to plot spatial transcriptomic data in Euclidean space.

Because spots in the spatial transcriptomic dataset may not correspond to cell boundaries, several additional features can be included when plotting on spatial domain. When the spatial transcriptomic measurement technology has a multicellular resolution, spots can be decomposed into constituent cell types. A 2D array of pie charts can be used to represent the cell types percentages of spots, as demonstrated in DSTG (79). To enable the investigation of cellular architecture at higher resolution, DSTG uses a GCN to uncover the cellular compositions within each spot. DSTG first leverages single-cell RNA-seq data to construct pseudo spatial transcriptomic (pseudo-ST) data by selecting two to eight single cells from the same tissue and combining their transcriptomic profiles. This pseudo-ST data is designed to mimic the cell mixture in the real spatial transcriptomic data and provide the basis for the model training. Via canonical correlation analysis, DSTG identifies a link graph of spots with the integration of the pseudo-ST data and the real spatial transcriptomic data. A GCN (74) iteratively updates the representation of each spot by aggregating its neighborhoods' information. The GCN model is trained in a semi-supervised manner, where the known cell compositions of the pseudo-ST nodes are served as the labeled data, and the real spatial transcriptomic nodes are the prediction targets.

While cell type deconvolution provides an estimation of cellular constituents, it does not directly increase the resolution of the dataset. BayesSpace uses a Bayesian model to increase the resolution to the subspot level, which approaches single-cell resolution with the Visium platform. The model specification is largely identical to the spatial domain detection model described above, except that unit of analysis is the subspot rather than the spot. Since gene expression is not observed at the subspot level, BayesSpace models it as another latent variable and estimates it using MCMC. The increase in resolution is different across measurement technology. For square spots (16), BayesSpace by default divides each spot into nine subspots. For hexagonal spots like Visium, they are divided into six subspots by default. The subspots can be visualized in Euclidean space similar to regular spots.

## 5 Analysis and visualization in the interaction domain

Cell signaling describes the process in which cells send, receive, process, and transmit signals within the environment and with themselves. Based on the signaling distance and the sender-receiver identities, cell signaling can be classified into autocrine, paracrine, endocrine, intracrine, and juxtacrine (80). It serves critical functions in development (81), immunity (82), and homeostasis (83) across all organisms. For example, the Hedgehog signaling pathway is involved in tissue patterning and orientation and aberrant activations of hedgehog signaling lead to several types of cancers (84). Single-cell datasets enable correlation analysis to unravel cell-to-cell interaction (85-87). Due to the lack of spatial information, single-cell analysis cannot distinguish short-distance (juxtacrine and paracrine) and long-distance (endocrine) signaling. Spatial transcriptomic datasets provide the spatial coordinate of each cell or spot and enable spatial dissection of cell signaling.

### 5.1 Cell-to-cell interaction

Cell signaling frequently occurs between cells in spatial proximity. Giotto takes spatial proximity into consideration to identify cell-to-cell interaction. It first constructs a spatial neighborhood network to identify cell types that occur in spatial proximity. Each node of the network represents a cell and pair of neighboring cells are connected through an edge. The neighbors of each cell can be determined by extending a circle of a predefined radius, by selecting the k-nearest neighbors, or by constructing a Delaunay network (88). Cell types connected in the network more than expected are considered interacting. Giotto permutes the cell type labels without changing the topology of the network, and calculates the expected frequencies between every pair of cell types. P-values are derived based on where the observed frequency falls on the distribution of expected frequencies.

Another method, SpaOTsc, leverages both single-cell and spatial transcriptomic data for a comprehensive profile of spatial interaction (34). It uses an optimal transport algorithm to map single-cell to spatial transcriptomic data. An optimal transport is a function that maps a source distribution to a target distribution while minimizing the amount of effort with respect to a predefined cost function (89). SpaOTsc generates a cost function based on the expression profile dissimilarity of shared genes across the single cell and the spatial transcriptomic datasets. The optimal transport plan maps single cells onto spatial locations. SpaOTsc then formulates cell-to-cell communication as a second optimal transport problem between sender and receiver cells. The expression of ligand and receptor genes are used to estimate sender and receiver cells, and the spatial distance is the cost function. The resultant optimal transport plan represents the likelihood of cell-to-cell communication.

## 5.2 Ligand-receptor pairing

Another aspect of cell signaling is the pairings between ligands and receptors. Giotto identifies ligand-receptor pairs whose mean expression is higher than expected. To obtain the observed expression of ligand-receptor pairs for a pair of cell types, Giotto averages the expression of ligand in all sender cells and the expression of receptors in all receiver cells in proximity of the sender cells. Giotto then permutes the location of cells to obtain an expected expression of the ligand-receptor pair. A p-value can be obtained by mapping the observed expression onto the distribution of expected expression.

Different from Giotto, SpaOTsc uses a partial information decomposition (PID) approach to determine gene-to-gene interaction. Intuitively, PID decomposes the mutual information between multiple source variables and a target variable into unique information contributed by each source variable, redundant information shared by many source variables, and synergistic information contributed by the combination of source variables (90). SpaOTsc estimates the unique information from a source gene to a target gene that is within a predefined spatial distance, taking into consideration all other genes.

## 5.3 Visualization of interactions between cells and genes

Cell-to-cell and gene-to-gene interactions are naturally represented as networks and correlation matrices (Figure 4). Integrative packages such as Giotto (76) provide functions to visualize cell-to-cell and gene-to-gene interactions as heatmaps, dot plots, or networks. A heatmap is a visual depiction of a matrix, whose values are represented as colored boxes on a grid. Using heatmaps, large blocks of highly connected cells or genes can be visually identified. A dot plot is similar to a heatmap, except that the boxes are replaced by dots of varying sizes. A dot plot can use both the size and the color of each dot to represent values in each interaction. Different from heatmaps and dot plots, networks use nodes to represent cells or genes and edges to represent their interactions. The widths and colors of edges can be used to describe the strength of interactions. Besides Giotto, the igraph package is widely adopted for network visualization and provides programming interfaces in R, python, C/C++, and Mathematica (91). Cytoscape is another widely used package to visualize complex network interaction. Its graphical user interface makes it easy to manipulate and examine nodes and edges in the network (92).

## 6 Discussions

Spatial transcriptomic technologies have made tremendous progress in recent years. Although earlier technologies are restricted by the number of profiled genes (9, 25, 26) or the spatial resolution (16), current methods can profile the whole transcriptome at single-cell or subcellular resolution (20-22). While available commercialized methods (Visium) cannot achieve cellular resolution, we believe newer technologies will soon be production-ready. As commercial platforms become more affordable,

we believe the speed at which spatial transcriptomic datasets becomes publicly available will only accelerate. For example, phase two of the Brain Initiative Cell Census Network (BICCN) will map the spatial organization of more than 300,000 cells from the mouse's primary motor cortex (93). Large-scale projects to comprehensively profile spatial gene expression are currently limited, but we envision that these projects will expand in three directions. First, more model organisms will be profiled, enabling comparative analysis of cell types and their spatial organizations across evolution. Second, more organ and tissue types will be profiled for a comprehensive understanding of spatial expression architecture. Third, cell states (e.g. stimulated vs. resting) and disease states (cancer vs. normal) will be profiled to understand cellular activation and disease pathology.

As spatial transcriptomic datasets become more abundant, meta-analysis across published datasets will become commonplace. Methods to remove batch effects are needed to account for technical confounders across datasets. Unlike bulk and single-cell sequencing, batch effects in spatial transcriptomic data must account for correlation across space. Further, the batch effect may also occur on companion histology images, and methods to jointly analyze histology image and spatial transcriptomic data are required. Although several methods have been developed for batch effect removal in bulk (94, 95) and single-cell (96, 97) sequencing, it is still an under-explored area for spatial transcriptomics.

Histopathology is widely adopted across a various domain of medicine, and is considered the gold standard for certain diagnoses such as cancer staging (98). However, histology is limited by the type and number of cellular features delineated by staining agents. Spatial transcriptomics extends histology to test for both imaging and molecular features, and may enable testing for oncogenic driver mutations critical for determining cancer subtypes. A recent method named SpaCell integrates both histology and spatial transcriptomic information to predict cancer staging (99). In this method, histological images are tiled into patches, where each patch corresponds to a spatial transcriptomic spot in a tissue. A convolutional neural network is used to extract image features from each patch, and combine the features with the spot gene count. A subsequent deep network is applied to predict the disease stages. We envision that spatial transcriptomics will become a diagnostic routine as it becomes more affordable and the clinical interpretation becomes more streamlined.

In this review, we surveyed state-of-the-art methods for spatial transcriptomic data analysis and visualization, and categorized them into three main categories according to the way their output is visualized. It is unlikely that we covered all available methods for spatial transcriptomics, but we hope this review will serve as a stepping stone and attract more researchers to this field.

## 7 Figure Captions

**Figure 1** Spatial transcriptomic datasets maps gene expression measurements to their respective locations (A). A spatial transcriptomic dataset can be analyzed in gene expression space, irrespective of spatial locations. Tasks such as clustering and cell type identification falls into this category (B). Spatial information can be used jointly with gene expression to detect spatial expression patterns and spatial domains (C). Further, these two sources of information can also be used to detect cell-cell and gene-gene interactions (D).

**Figure 2** Analysis and visualization in the gene expression space requires an input of gene-by-cell matrix (A). The gene dimension of the input matrix is reduced through dimensionality reduction techniques (B), and resulting matrix can be used for clustering (C). Marker genes of each cluster are identified and matched to known cell-type specific markers to identify cell types (D).

**Figure 3** To visualize gene expression in the Euclidean space, a matrix of spatial coordinates (x, y, and optionally z) is attached to the expression matrix (A). Spatially coherent genes (B) and spatial domains (C) can then be visualized as 2D images.

**Figure 4** Visualization of interactions requires a cell-by-cell or gene-by-gene correlation matrix (A). Visualization with heatmap and dot plot helps identify blocks of collected nodes (B), whereas network visualization helps identify hub nodes (C).

## 8 Conflict of Interest

We declare no conflict of interest.

## 9 Author Contributions

B.L. conceived the project. B.L. and Y.L. performed the literature review. B.L. and Y.L. wrote the paper.

## 10 Funding

We have no funding source to disclose.

## 11 Acknowledgments

We acknowledge Liang Zhang for providing helpful comments.

## 12 Reference

1. Asp M, Giacomello S, Larsson L, Wu C, Furth D, Qian X, et al. A Spatiotemporal Organ-Wide Gene Expression and Cell Atlas of the Developing Human Heart. *Cell*. 2019;179(7):1647-60 e19.
2. Rödelsperger C, Ebbing A, Sharma DR, Okumura M, Sommer RJ, Korswagen HC. Spatial transcriptomics of nematodes identifies sperm cells as a source of genomic novelty and rapid evolution. *Molecular Biology and Evolution*. 2021;38(1):229-43.
3. Chen WT, Lu A, Craessaerts K, Pavie B, Sala Frigerio C, Corthout N, et al. Spatial Transcriptomics and In Situ Sequencing to Study Alzheimer's Disease. *Cell*. 2020;182(4):976-91 e19.
4. Maniatis S, Aijo T, Vickovic S, Braine C, Kang K, Mollbrink A, et al. Spatiotemporal dynamics of molecular pathology in amyotrophic lateral sclerosis. *Science*. 2019;364(6435):89-93.
5. Berglund E, Maaskola J, Schultz N, Friedrich S, Marklund M, Bergenstrahlé J, et al. Spatial maps of prostate cancer transcriptomes reveal an unexplored landscape of heterogeneity. *Nat Commun*. 2018;9(1):2419.
6. Thrane K, Eriksson H, Maaskola J, Hansson J, Lundeberg J. Spatially Resolved Transcriptomics Enables Dissection of Genetic Heterogeneity in Stage III Cutaneous Malignant Melanoma. *Cancer Res*. 2018;78(20):5970-9.
7. Moncada R, Barkley D, Wagner F, Chiodin M, Devlin JC, Baron M, et al. Integrating microarray-based spatial transcriptomics and single-cell RNA-seq reveals tissue architecture in pancreatic ductal adenocarcinomas. *Nat Biotechnol*. 2020;38(3):333-42.

8. Ji AL, Rubin AJ, Thrane K, Jiang S, Reynolds DL, Meyers RM, et al. Multimodal Analysis of Composition and Spatial Architecture in Human Squamous Cell Carcinoma. *Cell*. 2020;182(6):1661-2.
9. Shah S, Lubeck E, Zhou W, Cai L. In Situ Transcription Profiling of Single Cells Reveals Spatial Organization of Cells in the Mouse Hippocampus. *Neuron*. 2016;92(2):342-57.
10. Moffitt JR, Bambah-Mukku D, Eichhorn SW, Vaughn E, Shekhar K, Perez JD, et al. Molecular, spatial, and functional single-cell profiling of the hypothalamic preoptic region. *Science*. 2018;362(6416).
11. Close JL, Long BR, Zeng H. Spatially resolved transcriptomics in neuroscience. *Nat Methods*. 2021;18(1):23-5.
12. Schwarzacher T, Heslop-Harrison P. Practical in situ hybridization: BIOS Scientific Publishers Ltd; 2000.
13. Metzker ML. Sequencing technologies - the next generation. *Nat Rev Genet*. 2010;11(1):31-46.
14. Gawad C, Koh W, Quake SR. Single-cell genome sequencing: current state of the science. *Nat Rev Genet*. 2016;17(3):175-88.
15. Shapiro E, Biezuner T, Linnarsson S. Single-cell sequencing-based technologies will revolutionize whole-organism science. *Nature Reviews Genetics*. 2013;14(9):618-30.
16. Stahl PL, Salmen F, Vickovic S, Lundmark A, Navarro JF, Magnusson J, et al. Visualization and analysis of gene expression in tissue sections by spatial transcriptomics. *Science*. 2016;353(6294):78-82.
17. Rodrigues SG, Stickels RR, Goeva A, Martin CA, Murray E, Vanderburg CR, et al. Slide-seq: A scalable technology for measuring genome-wide expression at high spatial resolution. *Science*. 2019;363(6434):1463-7.
18. Stickels RR, Murray E, Kumar P, Li J, Marshall JL, Di Bella DJ, et al. Highly sensitive spatial transcriptomics at near-cellular resolution with Slide-seqV2. *Nat Biotechnol*. 2021;39(3):313-9.
19. Vickovic S, Eraslan G, Salmen F, Klughammer J, Stenbeck L, Schapiro D, et al. High-definition spatial transcriptomics for in situ tissue profiling. *Nat Methods*. 2019;16(10):987-90.
20. Liu Y, Yang M, Deng Y, Su G, Enninfu A, Guo CC, et al. High-Spatial-Resolution Multi-Omics Sequencing via Deterministic Barcoding in Tissue. *Cell*. 2020;183(6):1665-81 e18.
21. Cho CS, Xi J, Si Y, Park SR, Hsu JE, Kim M, et al. Microscopic examination of spatial transcriptome using Seq-Scope. *Cell*. 2021;184(13):3559-72 e22.
22. Chen A, Liao S, Cheng M, Ma K, Wu L, Lai Y, et al. Large field of view-spatially resolved transcriptomics at nanoscale resolution. *bioRxiv*. 2021:2021.01.17.427004.
23. Eng CL, Lawson M, Zhu Q, Dries R, Koulena N, Takei Y, et al. Transcriptome-scale super-resolved imaging in tissues by RNA seqFISH. *Nature*. 2019;568(7751):235-9.
24. Lubeck E, Coskun AF, Zhiyentayev T, Ahmad M, Cai L. Single-cell in situ RNA profiling by sequential hybridization. *Nat Methods*. 2014;11(4):360-1.

25. Moffitt JR, Hao J, Wang G, Chen KH, Babcock HP, Zhuang X. High-throughput single-cell gene-expression profiling with multiplexed error-robust fluorescence *in situ* hybridization. *Proc Natl Acad Sci U S A*. 2016;113(39):11046-51.

26. Chen KH, Boettiger AN, Moffitt JR, Wang S, Zhuang X. RNA imaging. Spatially resolved, highly multiplexed RNA profiling in single cells. *Science*. 2015;348(6233):aaa6090.

27. Wang X, Allen WE, Wright MA, Sylwestrak EL, Samusik N, Vesuna S, et al. Three-dimensional intact-tissue sequencing of single-cell transcriptional states. *Science*. 2018;361(6400).

28. Lee J-H, Church GM. Highly multiplexed subcellular RNA sequencing *in situ*. *Science*. 2014;343(6177):1360-3.

29. Schermelleh L, Ferrand A, Huser T, Eggeling C, Sauer M, Biehlmaier O, et al. Super-resolution microscopy demystified. *Nat Cell Biol*. 2019;21(1):72-84.

30. Aird D, Ross MG, Chen WS, Danielsson M, Fennell T, Russ C, et al. Analyzing and minimizing PCR amplification bias in Illumina sequencing libraries. *Genome Biol*. 2011;12(2):R18.

31. Kim TH, Zhou X, Chen M. Demystifying "drop-outs" in single-cell UMI data. *Genome Biol*. 2020;21(1):196.

32. Crosetto N, Bienko M, van Oudenaarden A. Spatially resolved transcriptomics and beyond. *Nat Rev Genet*. 2015;16(1):57-66.

33. Svensson V, Teichmann SA, Stegle O. SpatialDE: identification of spatially variable genes. *Nat Methods*. 2018;15(5):343-6.

34. Cang Z, Nie Q. Inferring spatial and signaling relationships between cells from single cell transcriptomic data. *Nature communications*. 2020;11(1):1-13.

35. Wolf FA, Angerer P, Theis FJ. SCANPY: large-scale single-cell gene expression data analysis. *Genome Biol*. 2018;19(1):15.

36. Lun AT, McCarthy DJ, Marioni JC. A step-by-step workflow for low-level analysis of single-cell RNA-seq data with Bioconductor. *F1000Res*. 2016;5:2122.

37. Sun S, Zhu J, Zhou X. Statistical analysis of spatial expression patterns for spatially resolved transcriptomic studies. *Nat Methods*. 2020;17(2):193-200.

38. Kanungo T, Mount DM, Netanyahu NS, Piatko CD, Silverman R, Wu AY. An efficient k-means clustering algorithm: Analysis and implementation. *IEEE transactions on pattern analysis and machine intelligence*. 2002;24(7):881-92.

39. Reynolds DA. Gaussian mixture models. *Encyclopedia of biometrics*. 2009;741:659-63.

40. Johnson SC. Hierarchical clustering schemes. *Psychometrika*. 1967;32(3):241-54.

41. Blondel VD, Guillaume J-L, Lambiotte R, Lefebvre E. Fast unfolding of communities in large networks. *Journal of statistical mechanics: theory and experiment*. 2008;2008(10):P10008.

42. Traag VA, Waltman L, van Eck NJ. From Louvain to Leiden: guaranteeing well-connected communities. *Sci Rep*. 2019;9(1):5233.

43. Kaufman L, Rousseeuw PJ. *Finding groups in data: an introduction to cluster analysis*: John Wiley & Sons; 2009.

44. Love MI, Huber W, Anders S. Moderated estimation of fold change and dispersion for RNA-seq data with DESeq2. *Genome Biology*. 2014;15(12):550.

45. McCarthy DJ, Chen Y, Smyth GK. Differential expression analysis of multifactor RNA-Seq experiments with respect to biological variation. *Nucleic Acids Research*. 2012;40(10):4288-97.

46. Finak G, McDavid A, Yajima M, Deng J, Gersuk V, Shalek AK, et al. MAST: a flexible statistical framework for assessing transcriptional changes and characterizing heterogeneity in single-cell RNA sequencing data. *Genome biology*. 2015;16(1):1-13.

47. Dumitrascu B, Villar S, Mixon DG, Engelhardt BE. Optimal marker gene selection for cell type discrimination in single cell analyses. *Nat Commun*. 2021;12(1):1186.

48. Kim S-Y, Volsky DJ. PAGE: parametric analysis of gene set enrichment. *BMC bioinformatics*. 2005;6(1):1-12.

49. Subramanian A, Tamayo P, Mootha VK, Mukherjee S, Ebert BL, Gillette MA, et al. Gene set enrichment analysis: A knowledge-based approach for interpreting genome-wide expression profiles. *Proceedings of the National Academy of Sciences*. 2005;102(43):15545-50.

50. Littman R, Hemminger Z, Foreman R, Arneson D, Zhang G, Gómez - Pinilla F, et al. Joint cell segmentation and cell type annotation for spatial transcriptomics. *Molecular systems biology*. 2021;17(6):e10108.

51. Yuste R, Hawrylycz M, Aalling N, Aguilar-Valles A, Arendt D, Armañanzas R, et al. A community-based transcriptomics classification and nomenclature of neocortical cell types. *Nature neuroscience*. 2020;23(12):1456-68.

52. Roerdink JB, Meijster A. The watershed transform: Definitions, algorithms and parallelization strategies. *Fundamenta informaticae*. 2000;41(1, 2):187-228.

53. Wold S, Esbensen K, Geladi P. Principal component analysis. *Chemometrics and intelligent laboratory systems*. 1987;2(1-3):37-52.

54. Tsuyuzaki K, Sato H, Sato K, Nikaido I. Benchmarking principal component analysis for large-scale single-cell RNA-sequencing. *Genome Biol*. 2020;21(1):9.

55. McInnes L, Healy J, Melville J. Umap: Uniform manifold approximation and projection for dimension reduction. *arXiv preprint arXiv:180203426*. 2018.

56. Van der Maaten L, Hinton G. Visualizing data using t-SNE. *Journal of machine learning research*. 2008;9(11).

57. van den Heuvel M, Nusse R, Johnston P, Lawrence PA. Distribution of the wingless gene product in *Drosophila* embryos: a protein involved in cell-cell communication. *Cell*. 1989;59(4):739-49.

58. Lui JH, Hansen DV, Kriegstein AR. Development and evolution of the human neocortex. *Cell*. 2011;146(1):18-36.

59. Edsgard D, Johnsson P, Sandberg R. Identification of spatial expression trends in single-cell gene expression data. *Nat Methods*. 2018;15(5):339-42.

60. Wang J. An intuitive tutorial to Gaussian processes regression. *arXiv preprint arXiv:200910862*. 2020.

61. Gotway CA, Stroup WW. A generalized linear model approach to spatial data analysis and prediction. *Journal of Agricultural, Biological, and Environmental Statistics*. 1997:157-78.

62. McCullagh P, Nelder JA. Generalized linear models: Routledge; 1983.

63. Wedderburn RW. Quasi-likelihood functions, generalized linear models, and the Gauss—Newton method. *Biometrika*. 1974;61(3):439-47.

64. Breslow NE, Clayton DG. Approximate inference in generalized linear mixed models. *Journal of the American statistical Association*. 1993;88(421):9-25.

65. Fletcher CD. Diagnostic histopathology of tumors: 2-volume set with CD-ROMs: Elsevier Health Sciences; 2007.

66. Zhao E, Stone MR, Ren X, Guenthoer J, Smythe KS, Pulliam T, et al. Spatial transcriptomics at subspot resolution with BayesSpace. *Nat Biotechnol*. 2021.

67. Zhu Q, Shah S, Dries R, Cai L, Yuan GC. Identification of spatially associated subpopulations by combining scRNASeq and sequential fluorescence *in situ* hybridization data. *Nat Biotechnol*. 2018.

68. Blake A, Kohli P, Rother C. Markov random fields for vision and image processing: MIT press; 2011.

69. Li SZ. Modeling image analysis problems using Markov random fields. 2000.

70. Dempster AP, Laird NM, Rubin DB. Maximum likelihood from incomplete data via the EM algorithm. *Journal of the Royal Statistical Society: Series B (Methodological)*. 1977;39(1):1-22.

71. Moon TK. the expectation-maximization algorithm [Available from: <http://ieeexplore.ieee.org/stamp/stamp.jsp?tp=&arnumber=543975>].

72. Geyer CJ. Practical markov chain monte carlo. *Statistical science*. 1992:473-83.

73. Hu J, Li X, Coleman K, Schroeder A, Irwin DJ, Lee EB, et al. Integrating gene expression, spatial location and histology to identify spatial domains and spatially variable genes by graph convolutional network. *bioRxiv*. 2020.

74. Kipf TN, Welling M. Semi-supervised classification with graph convolutional networks. *arXiv preprint arXiv:160902907*. 2016.

75. Xie J, Girshick R, Farhadi A, editors. Unsupervised deep embedding for clustering analysis. International conference on machine learning; 2016: PMLR.

76. Dries R, Zhu Q, Dong R, Eng C-HL, Li H, Liu K, et al. Giotto: a toolbox for integrative analysis and visualization of spatial expression data. *Genome biology*. 2021;22(1):1-31.

77. Hao Y, Hao S, Andersen-Nissen E, Mauck III WM, Zheng S, Butler A, et al. Integrated analysis of multimodal single-cell data. *Cell*. 2021.

78. Palla G, Spitzer H, Klein M, Fischer D, Schaar AC, Kuemmerle LB, et al. Squidpy: a scalable framework for spatial single cell analysis. *bioRxiv*. 2021.

79. Song Q, Su J. DSTG: deconvoluting spatial transcriptomics data through graph-based artificial intelligence. *Briefings in Bioinformatics*. 2021.

80. Bradshaw RA, Dennis EA. *Handbook of cell signaling*: Academic press; 2009.

81. Wei C-J, Xu X, Lo CW. Connexins and cell signaling in development and disease. *Annu Rev Cell Dev Biol*. 2004;20:811-38.

82. Dustin ML, Chan AC. Signaling takes shape in the immune system. *Cell*. 2000;103(2):283-94.

83. Taguchi A, White MF. Insulin-like signaling, nutrient homeostasis, and life span. *Annu Rev Physiol.* 2008;70:191-212.

84. Taipale J, Beachy PA. The Hedgehog and Wnt signalling pathways in cancer. *nature.* 2001;411(6835):349-54.

85. Wirka RC, Wagh D, Paik DT, Pjanic M, Nguyen T, Miller CL, et al. Atheroprotective roles of smooth muscle cell phenotypic modulation and the TCF21 disease gene as revealed by single-cell analysis. *Nat Med.* 2019;25(8):1280-9.

86. Friedman CE, Nguyen Q, Lukowski SW, Helfer A, Chiu HS, Miklas J, et al. Single-Cell Transcriptomic Analysis of Cardiac Differentiation from Human PSCs Reveals HOPX-Dependent Cardiomyocyte Maturation. *Cell Stem Cell.* 2018;23(4):586-98 e8.

87. Krishnaswamy S, Spitzer MH, Mingueneau M, Bendall SC, Litvin O, Stone E, et al. Systems biology. Conditional density-based analysis of T cell signaling in single-cell data. *Science.* 2014;346(6213):1250689.

88. Chen L, Xu J-c. Optimal delaunay triangulations. *Journal of Computational Mathematics.* 2004;299-308.

89. Villani C. *Optimal transport: old and new:* Springer; 2009.

90. Kunert-Graf J, Sakhanenko N, Galas D. Partial Information Decomposition and the Information Delta: A Geometric Unification Disentangling Non-Pairwise Information. *Entropy.* 2020;22(12):1333.

91. Csardi G, Nepusz T. The igraph software package for complex network research. *InterJournal, complex systems.* 2006;1695(5):1-9.

92. Shannon P, Markiel A, Ozier O, Baliga NS, Wang JT, Ramage D, et al. Cytoscape: a software environment for integrated models of biomolecular interaction networks. *Genome research.* 2003;13(11):2498-504.

93. Marx V. Method of the Year: spatially resolved transcriptomics. *Nat Methods.* 2021;18(1):9-14.

94. Leek JT, Johnson WE, Parker HS, Jaffe AE, Storey JD. The sva package for removing batch effects and other unwanted variation in high-throughput experiments. *Bioinformatics.* 2012;28(6):882-3.

95. Stegle O, Parts L, Piipari M, Winn J, Durbin R. Using probabilistic estimation of expression residuals (PEER) to obtain increased power and interpretability of gene expression analyses. *Nature Protocols.* 2012;7(3):500-7.

96. Korsunsky I, Millard N, Fan J, Slowikowski K, Zhang F, Wei K, et al. Fast, sensitive and accurate integration of single-cell data with Harmony. *Nature methods.* 2019;16(12):1289-96.

97. Li X, Wang K, Lyu Y, Pan H, Zhang J, Stambolian D, et al. Deep learning enables accurate clustering with batch effect removal in single-cell RNA-seq analysis. *Nature communications.* 2020;11(1):1-14.

98. Edge SB, Byrd DR, Carducci MA, Compton CC, Fritz A, Greene F. *AJCC cancer staging manual:* Springer New York; 2010.

99. Tan X, Su A, Tran M, Nguyen Q. SpaCell: integrating tissue morphology and spatial gene expression to predict disease cells. *Bioinformatics.* 2020;36(7):2293-4.

Fig. 1

Spatial gene and spatial domain identification

Cell signaling and gene-gene interaction

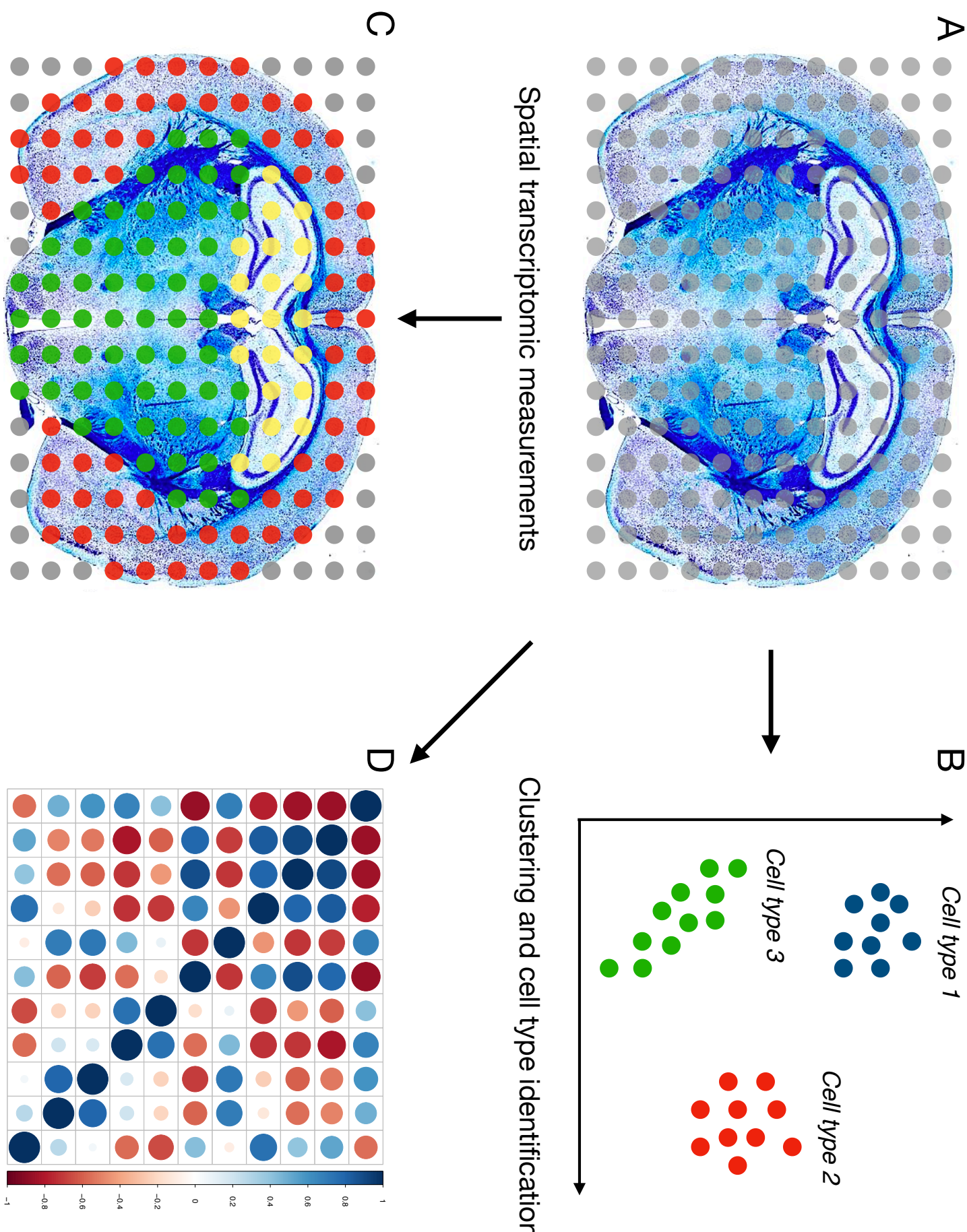
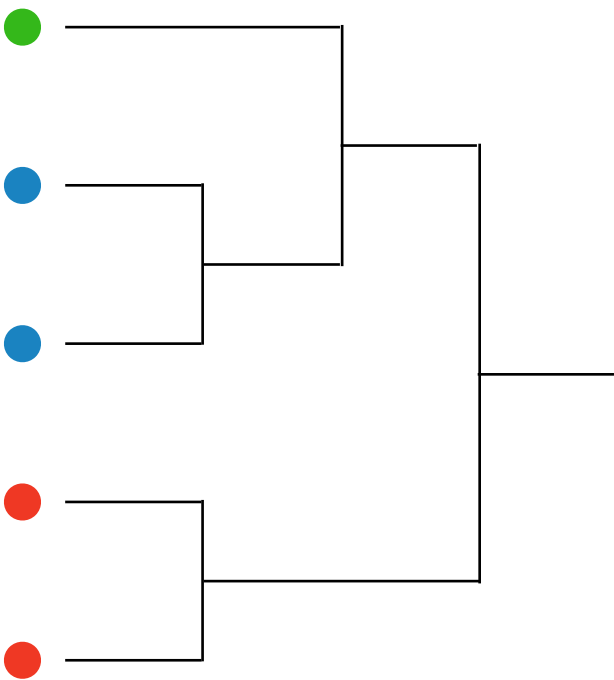


Fig. 2

Clustering



C

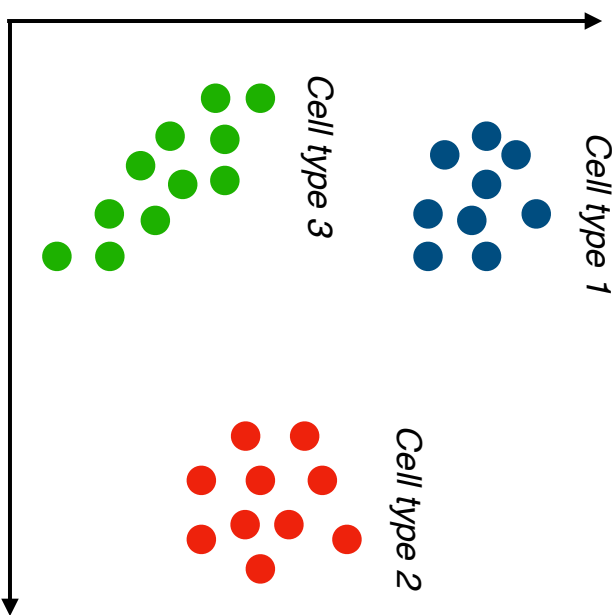
Input matrix

	Cell 1	Cell 2	Cell 3	...	Cell N
Gene 1	$X_{11}$	$X_{12}$	$X_{13}$	...	$X_{1N}$
Gene 2	$X_{21}$	$X_{22}$	$X_{23}$	...	$X_{2N}$
Gene 3	$X_{31}$	$X_{32}$	$X_{33}$	...	$X_{3N}$
...	...	...	...	...	...
Gene M	$X_{M1}$	$X_{M2}$	$X_{M3}$	...	$X_{MN}$

Dimensionality reduction

	Cell 1	Cell 2	Cell 3	...	Cell N
PC 1	$y_{11}$	$y_{12}$	$y_{13}$	...	$y_{1N}$
PC 2	$y_{21}$	$y_{22}$	$y_{23}$	...	$y_{2N}$
PC 3	$y_{31}$	$y_{32}$	$y_{33}$	...	$y_{3N}$
...	...	...	...	...	...
PC K	$y_{K1}$	$y_{K2}$	$y_{K3}$	...	$y_{KN}$

D

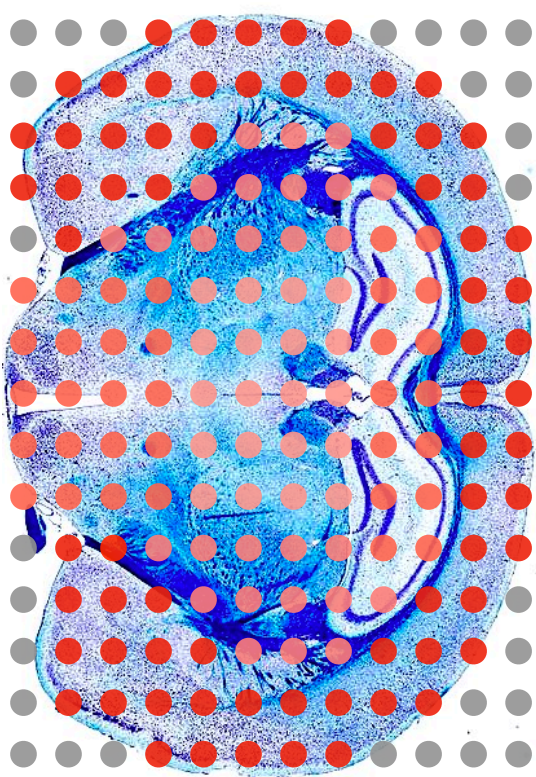
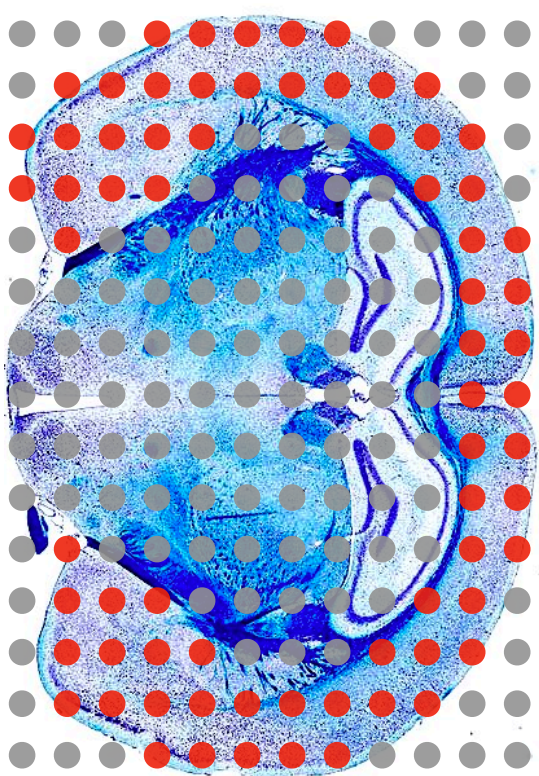


**Fig. 3****A**

Cell 1 Cell 2 Cell 3 ... Cell  $N$

 $X$  coord. $Y$  coord. $(Z$  coord.) $r_{x1} r_{x2} r_{x3} \dots r_{xN}$  $r_{y1} r_{y2} r_{y3} \dots r_{yN}$  $r_{z1} r_{z2} r_{z3} \dots r_{zN}$ 

Gene 1	$X_{11}$	$X_{12}$	$X_{13}$	...	$X_{1N}$
Gene 2	$X_{21}$	$X_{22}$	$X_{23}$	...	$X_{2N}$
Gene 3	$X_{31}$	$X_{32}$	$X_{33}$	...	$X_{3N}$
...	...	...	...	...	...
Gene $M$	$X_{M1}$	$X_{M2}$	$X_{M3}$	...	$X_{MN}$

**B****Spatially coherent gene****C****Input matrices****Spatially domain**

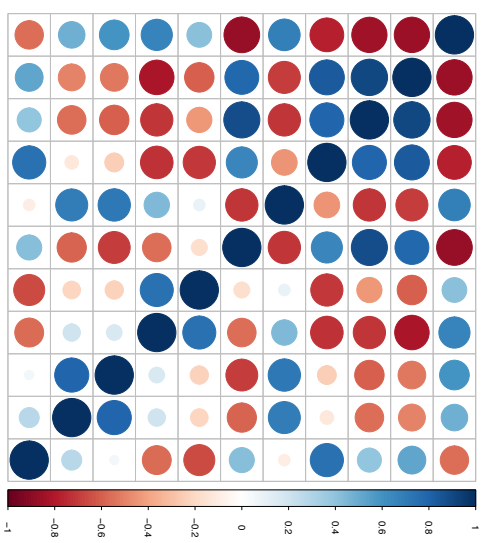
**Fig. 4**

**A**

	Cell 1	Cell 2	Cell 3	...	Cell N
Cell 1	$X_{11}$	$X_{12}$	$X_{13}$	...	$X_{1N}$
Cell 2	$X_{21}$	$X_{22}$	$X_{23}$	...	$X_{2N}$
Cell 3	$X_{31}$	$X_{32}$	$X_{33}$	...	$X_{3N}$
...	...	...	...	...	...
Cell N	$X_{N1}$	$X_{N2}$	$X_{N3}$	...	$X_{NN}$

Input matrix

**B**



Heatmap and dot plot

**C**

Network plot

